

**An approach towards continuous production of silver  
nanoparticle using *Bacillus thuringiensis***

Parth Sarthi Nayak<sup>a†</sup>, Manoranjan Arakha<sup>a†</sup>, Ajeet Kumar<sup>a</sup>, Shreyasi Asthana<sup>a</sup>, Bairagi C.

Mallick<sup>b</sup>, Suman Jha<sup>a\*</sup>

<sup>a</sup>Department of Life Science, National Institute of Technology Rourkela, Odisha  
769008, India.

<sup>b</sup>Department of Chemistry, Ravenshaw University, Cuttack, Odisha 753003,  
India.

<sup>†</sup>Authors shared equal contribution in the work.

## **Abstract**

Applying the principles of green chemistry for the synthesis of nanoparticles (NPs) is an emerging field of the current era. Continuous production of NPs, i.e. simultaneous bacterial growth and NPs production, if possible, would be more effective for different NPs mediated applications. Hence, our approach here is to optimize the method to produce and extract silver nanoparticle (AgNP) during growth of the bacteria, *Bacillus thuringiensis*. The fabricated AgNP was obtained when the bacteria were grown at minimum inhibitory concentration of AgNO<sub>3</sub> in culture medium. The microorganism produced elemental silver NP with particular surface physico-chemical properties pertaining to the cellular moieties acting as a capping agent. Fabrication of the NP was confirmed in UV-Vis absorbance spectra, attenuated total reflection fourier transform infrared spectra, zeta analysis, and field emission scanning electron micrographs. The UV-Vis and IR studies together indicated the presence of proteins on the NP surface. The fabricated NPs were further purified using size exclusion chromatograph (SEC), and the presence of NP in different elutions was further confirmed using the UV-Vis, IR spectroscopes, and TEM. The yield, upon purification, was 98.75 µg AgNP from 500 mL of the culture, which is relatively good yield. Additionally, the purified AgNP was found to have relatively stronger antibacterial activity against *Escherichia coli* than commercially available AgNP. The work shows that the microorganism with resistance to significant concentrations of metal ions can be used for continuous production of metal NPs for industrial as well as biological applications.

## 1. Introduction

The advanced physico-chemical properties of metal NPs make them unique entities compared to bulk materials for various biomedical and pharmaceutical applications<sup>1</sup>. Although, various physical and chemical methods are being optimized for engineering the metal NPs, still the biological methods have drawn attentions of different research groups working in this field to replace traditional physical and chemical methods, which frequently use toxic chemicals, and produce toxic wastes to the environment<sup>2-3</sup>. On the other hand, the biological methods, also known as green synthesis methods, are eco-friendly, safe, energy efficient, and less toxic than the other methods. Different biological agents have been used to fabricate the NPs such as plant extracts, extract from microorganisms and fungi<sup>2, 4</sup>. Engineering metal NPs using microbes have significant advantages like clean, non-toxic, eco-friendly, and it is also possible at ambient temperature and pressure<sup>5-6</sup>. In case of fabrication of metal NPs, the physico-chemical properties of the NPs are preserved by moieties acting as capping agents. The physico-chemical properties of metal NPs like magnetic property for iron NPs is lost upon air oxidation<sup>7</sup>, piezoelectric property of the ZnONPs is affected by variation in physico-chemical properties etc.<sup>8</sup>. Nevertheless, extraction, yield, and stability of metal NPs obtained through green synthesis has always been apprehended<sup>9-10</sup>.

Among different metal and metal oxide NPs, AgNP has drawn the attention of various research groups for various possible biological applications, such as nanomedicine, drug delivery, nanodevice fabrication, biosensing, catalysis, imaging<sup>11</sup>. AgNP synthesis by conventional methods involves chemical reduction in solution, sonochemical method, microemulsion method, and microwave assisted method<sup>12</sup>. AgNP prepared through these methods are very labile for rapid dissolution into Ag(I) ion on suspension in polar media like water, and causes toxicity to cells, unless the NP is capped with agents like TiO<sub>2</sub>, bacterial exopolysaccharides (EPS), biological moieties/biomolecules etc. The capping molecules

make the process of dissolution rate slower, resulting into longer half life of the particle <sup>13</sup>. Thus, AgNP productions by green synthesis methods have drawn attention of various research groups to avoid these problems. It is well reported that the biological entities, used for green synthesis of NPs, are enzymes and proteins which reduce metal ions into elemental metal crystals, and control size of the reduced metal crystals in nano-sizes, respectively <sup>14</sup>. In addition to the above reasons, bacterial growth rate and low maintenance conditions have drawn attention towards fabrication of metallic NPs using bacteria for various biological applications. The bacteria, growing in heavy metal rich environments, has also shown to have remarkable ability to reduce heavy metal ions, a property owing to its use for NP synthesis and for bioremediation of toxic metal ions <sup>15</sup>. Although, various studies have been done to decipher the extracellular and intracellular synthesis of AgNPs from different bacteria like *Pseudomonas stutzeri* <sup>16</sup>, *Bacillus subtilis* <sup>17</sup>, *Bacillus licheniformis* <sup>18</sup>, *Bacillus cereus* <sup>19</sup>, *Bacillus flexus* <sup>20</sup>, *Plectonema boryanum* <sup>21</sup>, and *Klebsiella pneumonia* <sup>22</sup>, but no studies have been done to obtain AgNPs from bacteria during their growth. Hence, we have taken an attempt to synthesize NPs during the growth of bacteria, and termed the process as ‘continuous production of NP’.

Ag(I) ion, because of toxic propensity, kills the bacteria at very low concentration that makes it very hard to use in live bacteria for AgNPs fabrication. However, bacteria with resistance to heavy metal ions or specifically growing in Ag(I) ion rich niche can be used for the purpose. In our recent study, we found resistance of *B. thuringiensis* to relatively very high concentration of Zn(II)/ZnONP <sup>23</sup>. Hence, in this study, we used same strain, relatively non-pathogenic *B. thuringiensis*, to fabricate AgNP. The fabricated AgNP was characterized using UV-Visible and attenuated total reflection fourier transform infrared (ATR-FTIR) spectroscopes, zeta analyzer, field emission scanning electron microscope (FE-SEM), and transmission electron microscope (TEM). Later the purification of fabricated AgNP from

bacterial culture was done using SEC. In addition to that, sodium hexametaphosphate (SHMP) was used in the mobile phase to avoid the irreversible binding of AgNP to the column, and for maintaining the monodispersivity of the NPs. However, antimicrobial study using LIVE/DEAD BacLight bacterial viability kit demonstrated relatively stronger antibacterial activity of fabricated AgNP compared to commercially available chemically synthesized AgNP from Sigma-Aldrich. Thus, the study optimized a novel and new green synthesis protocol for AgNP synthesis from commonly available non-pathogenic bacteria *B. thuringiensis*. Hence, the method can be adopted for continuous production of AgNP in bio-fermenter.

## **2. Experimental**

### **2.1. Materials and methods**

Nutrient broth and tannic acid were purchased from Himedia, India, whereas glutaraldehyde and sodium hexametaphosphate (SHMP) were purchased from Merck, India. Silver nitrate ( $\text{AgNO}_3$ ) and sephadex (G-100) were purchased from Sigma Aldrich. *Bacillus thuringiensis* (MTCC 8998) was procured from Institute of Microbial Technology, Chandigarh, India. All the formulations were prepared using deionised water, unless mentioned.

### **2.2. Minimum inhibitory concentration of $\text{AgNO}_3$ against *B. thuringiensis***

Initially, minimum inhibitory concentration (MIC) of  $\text{AgNO}_3$  against *B. thuringiensis* was optimized to fabricate AgNP. Briefly, *B. thuringiensis* mother culture was prepared by taking a loop full of bacteria from slant culture, and inoculated into nutrient broth followed by overnight incubation at 37 °C and 150 rpm orbital shaking. 50 mM  $\text{AgNO}_3$  stock solution was prepared by dissolving appropriate amount of  $\text{AgNO}_3$  in sterilized deionised water. Different reaction mixtures were prepared in 96-well plate, taking 20  $\mu\text{L}$  of mother culture in different  $\text{AgNO}_3$  concentrations, and the final volume was adjusted to 300  $\mu\text{L}$  using nutrient broth. Optical density at 600 nm was measured at regular time intervals for 24 hrs at 37 °C using micro-plate reader (Synergy H1 hybrid reader, Biotek, USA). MIC of 0.15 mM was

determined from the average optical density (O.D.) at 600 nm of three independent triplicate reactions at late log phase with approximately 42 % of the O.D. compared to the O.D. of untreated bacterial growth (Fig. 1 (a)).

### **2.3. Bacterial viability at MIC value**

The MIC value was further confirmed qualitatively as well as quantitatively by conducting fluorescence microscopic study using LIVE/DEAD BacLight assay. The LIVE/DEAD BacLight viable kit (L7007, Molecular probes, Invitrogen) was used to distinguish the viable cells from non-viable cells<sup>23-24</sup>. Briefly, 30 mL of *B. thuringiensis* culture was prepared by inoculating 1 mL of overnight culture and adding 0.15 mM AgNO<sub>3</sub>, and allowed to grow up till the end of log phase. Another 30 mL culture without AgNO<sub>3</sub> was also prepared for positive control. From each culture, 25 mL of the culture was centrifuged at 7000 rpm for 15 minutes. The pellet was collected, and resuspended in 2 mL of HEPES buffer (10 mM, pH 7.4, containing 150 mM NaCl). 1 mL of the *B. thuringiensis* cell suspension was added to 20 mL of HEPES buffer in a separate tube. The sample was incubated (mixing at every 15 minute interval) for one hour at room temperature. The cells were washed two times with HEPES buffer by centrifuging and resuspending the pellet in 20 mL HEPES buffer. Finally, the pellet was resuspended in 10 mL HEPES buffer, and O.D. was measured at 670 nm. 3 µL of dye mixture was added to 1 mL of the above samples and incubated for 15 minutes in the dark, followed by imaging using a fluorescence microscope (Olympus IX71, Germany) with 20x objective lens.

### **2.4. Biosynthesis and purification of AgNP from *B. thuringiensis***

From the MIC measurement, the AgNO<sub>3</sub> MIC against *B. thuringiensis* was found at 0.15 mM, which was also further confirmed by the LIVE/DEAD BacLight assay. Hence, 0.15 mM AgNO<sub>3</sub> was considered for synthesis of AgNP during the bacterial growth in the culture medium. For the AgNP synthesis, 1 mL of *B. thuringiensis* mother culture was added in 500

mL of nutrient broth, and incubated at 37 °C, 150 rpm agitation. Upon reaching the mid log phase of growth, the culture was supplemented with AgNO<sub>3</sub> to attain final concentration of 0.15 mM in the respective culture medium. The resulting culture was further incubated in the same conditions for additional 24 hrs to get reduced elemental silver nanocrystals.

Bacterial culture containing reduced elemental silver nanocrystals was centrifuged at 6000 rpm for 30 minutes, followed by pellet collection, and resuspension of the pellet into 10 mL of deionised water. The suspension was sonicated for 30 minutes (at 80 amplitude) to disrupt the bacterial cell membrane, thus the intracellular NP came in cell lysate. The suspension containing lysate was again centrifuged at 12000 rpm for 30 minutes, and the supernatant was collected and filtered using 0.22 µm cut-off membrane filter. The filtered supernatant containing NP was stored at 4 °C for further analysis. The AgNP from the above supernatant was further purified by SEC using 15 mL of sephadex G-100 resin soaked and washed with deionised water, and 10 mM sodium hexametaphosphate (SHMP) suspended in deionised water was taken as mobile phase with a flow rate of 1 mL/minute.

## **2.5. Characterization of AgNP**

AgNP sample collected before and after SEC were analyzed using different biophysical techniques. The surface plasmon resonance property of AgNP was analyzed using UV-Vis spectrophotometer (Cary 100, Agilent Technology, Singapore), whereas stability of NPs was analyzed depending on the surface potential values measured using the zeta analyzer (Malvern Zetasizer, Nano ZS90, Netherland). The bond level characterization of possible molecules responsible for reduction of Ag (I) into elemental Ag (0) and AgNP fabrication was done using ATR-FTIR spectroscope (Alpha ATR-FTIR, Bruker, Germany). The bond vibrations were measured putting sample over diamond platform with 128 scans at 2 cm<sup>-1</sup> resolutions in the range of 2000 - 500 cm<sup>-1</sup>.

To check the morphology of fabricated AgNP, the bacterial samples from the early stationary phase of bacterial growth kinetics in absence and presence of 0.15 mM AgNO<sub>3</sub> was taken for FE-SEM (Nova Nano SEM 450, FEI company) analysis. The bacterial sample taken for FE-SEM analysis was properly fixed using glutaraldehyde and tannic acid, as described in the published literature<sup>23</sup>. However, 10 µL of SEC elutions were directly put on glass slide for the imaging without any fixing. Both kind of the samples were scanned at 10 kV accelerating voltage after gold coating for 3 minutes. For TEM imaging, the SEC load and elutions (1-4) were centrifuged at 12000 rpm for 45 mins, 4 °C. The pellet were resuspended in deionised water prior to coating on carbon grid. The grids were scanned for AgNPs using TEM (FEI Tecnai TF20, Netherland).

Additionally, the concentration of fabricated AgNP after SEC was determined by atomic absorption spectrophotometer (Perkin Elmer AA200, Singapore) using a specified cathode lamp with corresponding wavelength. Before measuring the samples, the flame absorptions were calibrated using respective standard solutions in the range of 1-2 mg/mL.

## **2.6. Antibacterial activity of purified AgNP**

The LIVE/DEAD baclight viability assay is one of the important methods to study the antimicrobial activity of various NPs. The impact of AgNP on *E. coli* was studied using LIVE/DEAD Baclight viability kit (L7007, Molecular probes, invitrogen) with the help of fluorescence microscope with 20X objective lens, as mentioned above. The samples were prepared for fluorescence microscope following the protocol as described above. For a comparative analysis, we have taken commercially available AgNP (product code-730785, Sigma Aldrich, USA) as a standard, and prepared the samples following the protocol, maintaining the concentration of both AgNP at 9.2 µg/mL.

## **Results and discussion**

### **3.1. MIC of AgNO<sub>3</sub> against *B. thuringiensis***

As expected, the bacteria show significant resistance to Ag (I) ion. From the growth kinetics, when the O.D. at 600 nm from the stationary phase was plotted against AgNO<sub>3</sub> concentration, MIC of 0.15 mM was observed (Fig. 1a). However, the kinetic experiment was performed in triplicate to further strengthen the observation. The spectroscopic data were further supported by microscopic data, the Backlight assay performed at MIC concentration, i.e. at 0.15 mM AgNO<sub>3</sub>. Interestingly, the bacterial population was equally populated with viable and non-viable cells, when they were grown at the MIC. The viable cells with intact membrane are stained green by syto9 dye fraction present in mixture of dyes used in the Backlight assay (Fig. 1b-I). On the other hand, non-viable cells with depolarized membrane are stained red by the propidium iodide dye fraction present in the mixture of the dyes (Fig. 1b-II)<sup>23</sup>. However, in figure 1b-II there are relatively small, but significant, numbers of cells which have co-localized dyes. The finding can be rationalized either of the co-localized/overlaid viable and non-viable bacterial cells during slide preparation, or the cells undergoing viable to non-viable phase transition within the reading time frame (transient cells). Nevertheless, the population fractions shared by viable, non-viable and transient cells exist as 40:40:20 at the scale of 100 (Fig. 1b-II), which clearly strengthen the MIC value concluded from the growth kinetics experiment (Fig. 1a).

Silver ion is a well-known antimicrobial agent. It interacts with sulphur containing proteins present in cell wall and/or in cytoplasm, resulting into non-availability of the protein functions<sup>13</sup>. That is not the only possible method by which silver triggers the non-viability of bacterial strains. The presence of silver ions also disrupt the electrochemical gradient in bacterial inter-membrane space leading into non-viable cells. Additionally, the presence of silver ions in culture also result in enhanced level of reactive oxygen species (ROS) that can also cause the cell death through membrane depolarization<sup>13</sup>. However, certain bacteria during the evolutionary screening adopted approaches like efflux pumps (*Bacillus pumilus*),

reduction of toxic silver ion into non-toxic elemental silver (*Pseudomonas stutzeri* AG259) etc., which helped them to fight back against Ag(I) ion toxicity or to grow in silver rich environment <sup>13</sup>. In the later case, the bacterium has a protein that is very specific for the silver ion, i.e. it has the silver-binding motif, AgBP2. The protein with the motif binds, and helps them to reduce into non-bioavailable elemental silver crystals up to 200 nm of size <sup>13</sup>. However, the interaction between silver ion and silver ion specific proteins plays important role determining the fate of bacteria upon interaction with silver ion. As reported, the toxicity of silver ion is closely related to the interaction of silver ion with thiol (sulfhydryl) group <sup>25-26</sup>. Hence, the protein containing amino acids like cysteine strongly interact with silver ions and neutralize the silver ions using reducing biological process to rescue the Ag(I) dependent cell death. On the other hand, it is very interesting to note that amino acids with disulfide bonds and non-sulphur containing amino acids are totally unable to neutralize the silver ions against the bacteria <sup>25</sup>. Hence, the bacterial protein plays very important role in determining the toxicity of silver ions.

In recent work on metal oxide NPs, we found that *B. thuringiensis* is relatively resistant to the NP and the respective metal ions that are formed upon the NP suspension into the culture <sup>23</sup>. Hence, the bacterial resistance against metal ion and metal oxide NP is used for this work to reduce the silver ions into elemental silver nanocrystals during the growth of the bacteria <sup>27-29</sup>.

### **3.2. Validation of the approach as a continuous process**

The primary aim of this study was to establish a platform for large scale production of NPs, which will boost different industrial applications of the NP. Many research groups <sup>4-5, 30-31</sup> have already established the synthesis protocol (both chemical and green synthesis) for production of AgNP. However, most of the green synthesis protocols are based on batch culture techniques, using the bacterial cell mass in which AgNP production depleted after

certain time interval, hence compromises the industrial level applications of AgNP. Here, we have taken a step to create a platform for large scale production of AgNP. The process was termed as ‘continuous production’ and we hypothesized that this study will be helpful for large scale production of many NPs by adopting the protocol in biofermentor. To prove the process as continuous, we performed three batch cultures by inoculating the culture with previous culture (detail method in ESI). The synthesis of AgNP in each cultures was confirmed from the UV-Vis spectra (Fig. 2a), where SPR peak was found at 414 nm, and from the IR peaks within 800-500  $\text{cm}^{-1}$  for Ag-Ag and/or Ag-O vibration (Fig. 2b). Additionally, the number of live cells at the stationary phase (harvesting point) was evaluated using the BacLight viability assay, where we found more than 50 % live cells in each cultures. Additionally, the fig. 2a and 2b confirmed the synthesis of AgNP in all the three cultures, while fig. 3a, b, and c confirmed the presence 53 %, 64 %, and 60 % of viable cells in first, second, and third batch cultures, respectively. However, the live cells found at the end of the third batch culture can be used, further, for next batch culture to obtain AgNP. The enhanced viability from culture 1 to next cultures is dedicated to the propagation of Ag(I) ion tolerant fraction in the cultures. To this end, if the approach is adopted in biofermenter, harvesting 90-95 % of the culture after 24 hrs of incubation, and supplementing 10-5 % of remaining culture with fresh media of equal volume containing 0.15 mM Ag(I) ion for next harvest after 24 hrs of incubation can be done for optimum continuous production of AgNP. Hence, the findings clearly demonstrate that the protocol can be adopted in biofermentor for large continuous production of AgNP.

### **3.3. Fabrication of AgNP**

During the green synthesis of NPs using both plants as well as microorganisms, the moieties attached to the NP interface may vary from proteins to phytochemicals present in cells. The moieties are responsible in either reducing the metal ion into elemental metal or capping the

size of elemental metal by reducing the free energy content upon the interactions. In both the cases, molecules attached to NP surface are called nanoparticle corona, which consists of loosely attached layer (soft core) and tightly attached layer (hard core) of the corona<sup>32</sup>. Here, the fabrication of AgNP by different biomolecules was confirmed from UV-Vis and ATR-FTIR spectroscopic analysis.

According to Schmid, F.X., the peptide groups present in the protein main chain have potentials to absorb strongly the far-UV light in range of 180-230 nm, whereas the side chains of aromatic amino acids like Tyr, Trp and Phe absorb in near-UV region of 240-300 nm<sup>33</sup>. It is very interesting to observe the UV-Vis spectra of AgNP samples, where we got absorbance maxima in between 215-247 nm along with the shoulder at ~ 280 nm (Fig. 4). The data provide a clear indication of the presence of proteins in AgNP samples. Moreover, as shown in fig. 4, these findings remain unchanged for AgNP containing elution samples obtained after SEC. Additionally, the result is also supported by IR (amide I and II band peaks in the range of 1650 and 1545  $\text{cm}^{-1}$ ) and zeta potential results (Fig. 8 and table 1, respectively), as well as the SDS-PAGE (sodium dodecyl sulfate polyacrylamide gel electrophoresis) analysis as described in electronics supplementary information (Fig. S1, ESI). The missing protein band or the protein band with lesser intensity than control in SDS-PAGE (Fig. S1, ESI), confirmed the respective proteins are strongly attached to AgNP surface forming nanoparticle corona.

Based on the experimental results, we proposed a mechanism of AgNP synthesis from silver ions inside bacterial cells, and represented in the schematic diagram (Scheme 1). Here, we have divided the whole process into two important events, (i) reduction of Ag(I) into elemental silver Ag(0), and (ii) capping or ceasing of reduced silver element growth into nanocrystal sizes by biomolecules, preferably by proteins present in the cell. In the first step, proteinaceous enzymes act as a reducing agent to convert Ag(I) ion into elemental Ag(0). In

the step, Ag(I) ion enter into the bacterial cell via different membrane channels called porins or diffuse because of differential electromotive forces, followed by the reduction of Ag(I) ion into metallic Ag(0) by accepting electron from NADH to NAD<sup>+</sup> conversion<sup>34</sup>. The conversion is assisted by thiol containing proteins, which generally have relatively higher binding potential for Ag(I) ion<sup>25</sup>. Absence of reducing (neutralizing) propensity in protein causes bacterial cell death, since the binding protein will not be available for the biological functions<sup>25</sup>. Hence, the reduction is possible by NADH dependant reductase enzymes, only.

In the second step, nanoparticle-protein interactions play a vital role in stabilizing the growth of elemental silver crystals in nanometre sizes, hence the nanocrystal or nanomaterial is formed. The fabricated NP are capped by the Ag(0) specific or metal specific bacterial proteins, as discussed for the bacteria, *P. stutzeri* AG259<sup>13</sup>. The proteins bind to the growing elemental crystals, and stabilize the growth in nanometre-size crystals. Because of the loosely attached moieties upon the nanoparticle surface, the hydrodynamic size of the particle is relatively higher with significant deviation from standard nanoparticle size (Fig. 5). However, some of the protein capped NPs are secreted out to the bacterial surface via exocytosis/cellular efflux system<sup>28-29</sup> or other processes, and remain suspended in the bacterial culture or remain attached on the surface of bacterial membrane as shown in FE-SEM image (Fig. 6b). Generally, NPs present in supernatant or outside the cells are very dilute, having very low concentrations, thus the yield. To avoid the problem, the cells are lysed to harvest relatively higher NP concentration. However, the optimized method, here, can be adopted in bio-fermenter to get the NPs at the industrial scale using *B. thuringiensis* or *Pseudomonas stutzeri* AG259 or similar kind of bacteria, which will also sort out the problem of lower yield of the NPs through green synthesis methods.

### **3.4. Characterization of synthesized AgNP**

#### **3.4.1. UV-Vis spectroscopic analysis**

After the fabrication of AgNP, the mixture of cellular moieties with AgNP was further purified using SEC, in which 10 mM SHMP was used as anti-agglomerating agent in mobile phase for the SEC<sup>35</sup>. Like the molecules with polymeric charges, SHMP upon adsorption at the interface provides negative surface potential, resulting into monodispersivity of the particles, hence the stability. Initially, the reduced elemental AgNP was characterized by observing the UV-Vis spectra after three times dilution of the sample. The peak at 413 nm (Fig. 4, inset), arising due to surface plasmon resonance property of AgNP, confirmed the fabrication of AgNP. The peak value is very close to the value obtained by different scientific groups for AgNP<sup>3, 6</sup>. Interestingly, the absorbance peaks for both AgNPs before and after purification were found at 413 nm, which confirms that SEC elutions (elutions 1-5) has purified the AgNPs from non-conjugated moieties present in the suspension without any significant effect on SPR of AgNPs. However, the peaks for successive elutions (elution 4 and 5) became less intense, and finally become flat around 413 nm indicating that the AgNP population decreases with successive elution. The elution was further collected for 5 column volumes (100 mL of total elutions volume) without any further peak around 413 nm, indicating no further AgNPs on column.

The photocatalytic activity of metal NPs depends on the band gap energy of NPs, i.e. lower the band gap energy, higher the photocatalytic propensity. Here, the band gap energy of synthesized AgNP is evaluated from UV-Visible spectra using the equation,  $E_{bg} = 1240/\lambda$  (eV)<sup>23</sup>, where  $E_{bg}$  is the band gap energy in eV and  $\lambda$  is the cut off wavelength (absorbance peak) in nanometre. For the fabricated AgNP, the band gap energy ( $E_{bg}$ ) before and after purification are found to be 3.00 eV, which is closest to the cited value in literature, 2.6 eV<sup>31, 36</sup>.

### **3.4.2. Hydrodynamic size and surface potential analysis**

The hydrodynamic sizes of AgNP were evaluated by zeta analyser, as represented in fig. 5. As shown in the figure, the average hydrodynamic size of the AgNP before SEC was 152 nm with standard deviation of +/- 90 nm, confirming the presence of polydispersed particles like nanoparticles, cellular moieties etc. Interestingly, after purification using SEC, hydrodynamic size as well as the deviation from size reduced with each successive elution. The reduction in size, in case of nanoparticle, is rationalised to the removal of soft-corona during the purification. Moreover, the reduction in dispersivity or standard deviation is because of separation of cellular moieties with very large size differences upon SEC. Hence, it can be concluded that the purification by SEC is more effective than centrifugation. The SEC dependent purification can further be optimized by selecting respective pore size resins for the method, and can be efficiently used as an alternative of ultracentrifuge dependent separation of different size nanoparticles or nanoparticle from non-conjugated cellular moieties. Additionally, the zeta potential study along with size measurement helped in evaluating the additional importance of SEC. Initially, the zeta potential measurement of the samples (before SEC) indicated the polydispersivity nature of fabricated AgNP along with the presence of other cellular moieties with very large surface potentials. AgNP has negative surface potential, as cited in literatures also <sup>37-38</sup>.

The presence of negative surface potential in our data (table 1) confirms the presence of AgNP and the cellular moieties with negative surface potentials. The data suggests that along with negative value (26 %), there is presence of some particles that contribute to the positive surface potential (~74 %). The data confirmed that the moieties may be proteins or other cellular moieties or both with positive surface potentials. However, the significant improvement in dispersivity was observed with successive elutions. For example in elution 1, we observed presence of 52.6 % positive and 47.4 % negative surface potentials, and this is due to the collection of molecules larger than the pores of size exclusion resin. Molecules

larger than the pores of the resin pass through the void volume of the gel. Interestingly, in elution 2, 99.5 % negative surface potential was found which is due to the presence of relatively pure AgNP. The AgNP fraction in elution 2 moved through the largest pores of the resin, and eluted after the first elution. The elution 2 has only fabricated AgNP, as confirmed by UV-Visible spectra. However, with successive elutions, the fraction of positive surface potential increased and negative surface potential decreased. The change in fraction composition is due to the elution of smaller cellular moieties with respective surface potentials along the traces of smaller AgNPs.

### **3.4.3. Morphological analysis of fabricated AgNP**

The morphological features of fabricated AgNP were further explored using FE-SEM and TEM. As shown in fig. 6, the FE-SEM image indicates the rod shape morphology of *B. thuringiensis* with smooth surface (Fig. 6a), and spherical like molecule attached to the surface of the bacteria (Fig. 6b), indicating the fabricated AgNP over the surface of *B. thuringiensis*. The sample for FE-SEM was taken from the early stationary phase of the bacteria grown in presence of 0.15 mM AgNO<sub>3</sub>. Hence, the image (Fig. 6b) indicates that the NPs are being fabricated as the bacteria grow, and are secreted outside of the cells. Moreover, from the analysis of FE-SEM image, the surface morphology of fabricated AgNP after SEC was found to be spherical in shape with an average diameter in the range of 10 to 30 nm (Fig. 6c). Sizes of the particle obtained using FE-SEM was further supported by images acquired using TEM. Images obtained using TEM (Fig. 7) indicated the presence of particle with size 10-30 nm in SEC load (sample before SEC, Fig. 7a). However, the varying sizes of the particle, as shown in the figure, separated with the successive elutions (Fig. 7b-d). Additionally, the presence of the nanoparticle in elutions also reduced to beyond the detection limit by elution 4, with optimum population in elution 2. The finding further supports the

UV-Visible spectra and Zeta potential data. Hence, fig. 7 represents the TEM images of particles found in the samples, before SEC to elution 3.

The particle size found using TEM or FE-SEM is smaller than the hydrodynamic size observed using Zeta sizer. The difference in size can be dedicated to the sample preparation and the principles followed by the techniques. FE-SEM, in general, gives particular field image of the nanoparticles, but Zeta sizer measures the hydrodynamic size of the particles in respective medium, and gives the average of the particles coming in the light path, i.e. average size of the predominant particle population. However, in solution, the particle size varies significantly because of the absorption of the moieties to different extent, to lower the free energy content. Hence, the zeta sizer indicated fivefold higher the size than the size observed in images collected using FE-SEM/TEM. The data altogether indicate that *B. thuringiensis* when grown in presence of 0.15 mM AgNO<sub>3</sub>, reduces the Ag(I) ion into elemental silver nanocrystals with average size of 10-30 nm diameter, and the NPs are secreted outside of the cell along with the protein corona, like in *Pseudomonas stutzeri* AG259<sup>13,26</sup>.

#### **3.4.4. Bond level characterization of AgNPs**

The bond level characterization of both AgNP samples before and after SEC was done by ATR-FTIR spectra. As shown in fig. 8, the absorption peaks at 564 cm<sup>-1</sup> before SEC, and at 546, 523, 550, and 564 cm<sup>-1</sup> for different SEC elutions confirmed the presence of Ag-Ag/Ag-O bond vibrations, hence confirming the presence of AgNP in the solutions<sup>23</sup>. The strong absorption peaks at 1644 cm<sup>-1</sup> is due to the C=O vibrations (amide I) and at 1549 cm<sup>-1</sup>, 1520 cm<sup>-1</sup> are due to the N-H vibrations (amide II) confirming the presence of proteins in the eluted samples. Protein(s) present in the eluted samples are either part of the nanoparticle corona (hard or soft corona) or present in bulk solution in equilibrium with the protein(s) present in corona or both. Here, the proteins are either reducing the Ag (I) ions to AgNP or

acting as a capping agent or both. It has been reported that proteins can bind to NP either through free amine groups, cysteine and hydroxide groups present in proteins resulting into reduction of the particles free energy content, thereby stabilizing NP<sup>39-41</sup>. Additionally, strong peak at  $\sim 1114 \text{ cm}^{-1}$  for all the elutions indicated the presence of SHMP on NP interface as well as in the bulk solution. Additionally, upon purification using SEC, the concentration of AgNP, 9.875 ppm or 9.875  $\mu\text{g/mL}$ , was observed by atomic absorption spectroscope.

### **3.5. Antimicrobial activity of purified fabricated AgNP**

The antibacterial activity of biofabricated AgNP was evaluated using LIVE/DEAD BacLight bacterial viability fluorescence Kit. According to the assay, when bacterial cells are stained with this dye, show green fluorescence for the live cells with intact membrane, or red for dead cells with deformed membrane. Hence, it is considered as a suitable dye to study antimicrobial activity, which gives both qualitative and quantitative analysis of antimicrobial activity. The fig. 9a and 9b show the fluorescence images of intact and purified AgNP treated *E. coli* cells. A statistical analysis using imageJ<sup>42</sup> software reveals that the control of *E. coli* contains 100 % green cells, interpreting 100 % live cells, whereas purified AgNP treated *E. coli* culture contains a mixture of green ( $\sim 45\%$ ) and red cells ( $\sim 55\%$ ) (Fig. 9b). The result indicated that the presence of 9.2  $\mu\text{g/mL}$  of fabricated AgNP in *E. coli* culture reduced the viability of the bacterium to 45 %, only. A comparative analysis with commercially available AgNP from sigma (Fig. S2, ESI) revealed that the fabricated AgNP has relatively stronger antibacterial activity. The stronger antimicrobial activity of the fabricated AgNP can be attributed to additive effects of the nanoparticle corona and the nanoparticle.

## **4. Conclusion**

The study optimized the protocol to fabricate metallic NP using live *B. thuringiensis*, and purified the NP in stable form. The NP obtained was spherical in shape with 5-30 nm

diameters. The yield of the nanoparticle (pure) obtained is 98.75 µg from 500 mL of the bacteria culture. Protein(s) present in nanoparticle corona played important role in bioreduction of Ag(I) ion into AgNP, and its dispersivity. The purified AgNP showed relatively stronger antibacterial activity against *E. coli* than the commercially available AgNP. The optimized process of obtaining eco-friendly, cost effective, and fabricated AgNP can be used for large-scale production by adopting the protocol in the bio-fermenter.

### **Acknowledgments**

We are thankful to the Department of Ceramic Engineering, National Institute of Technology Rourkela, Odisha, India, for providing the FE-SEM facility for fulfilment of the research work. We are also thankful to Dr. Mamata Mohapatra, Department of Hydro & Electrometallurgy, Institute of Minerals and Material Technology, Bhubaneswar, Odisha, India, for providing the AAS facility. Additionally, we are also thankful to Dr Manidipa Banerjee, Kusum School for Biological Sciences, Indian Institute of Technology Delhi, for the image acquisition using T.E.M. facility. For the financial support, we will like to acknowledge the Department of Science and Technology, Department of Biotechnology, and the Ministry of Human Resource and Development, Govt. of India, India.

### **References**

1. M. J. Ahmed, G. Murtaza, A. Mehmood and T. M. Bhatti, *Materials Letters*, 2015, 153, 10-13.
2. H. Duan, D. Wang and Y. Li, *Chemical Society Reviews*, 2015, 44, 5778-5792.
3. P. Banerjee, M. Satapathy, A. Mukhopahayay and P. Das, *Bioresources and Bioprocessing*, 2014, 1, 1-10.
4. S. Behera, S. Jha, M. Arakha and T. Panigrahi, *IJERA*, 2013, 3, 058-062.
5. V. L. Das, R. Thomas, R. T. Varghese, E. Soniya, J. Mathew and E. Radhakrishnan, *3 Biotech*, 2014, 4, 121-126.
6. C. Malarkodi, S. Rajeshkumar, K. Paulkumar, G. Gnanajobitha, M. Vanaja and G. Annadurai, *Nanosci. Nanotechnol*, 2013, 3, 26-32.
7. M. Arakha, S. Pal, D. Samantarrai, T. K. Panigrahi, B. C. Mallick, K. Pramanik, B. Mallick and S. Jha, *Scientific reports*, 2015, 5, 14813.
8. M. Mahdavi, M. B. Ahmad, M. J. Haron, F. Namvar, B. Nadi, M. Z. A. Rahman and J. Amin, *Molecules*, 2013, 18, 7533-7548.
9. S. K. Balasubramanian, L. Yang, L.-Y. L. Yung, C.-N. Ong, W.-Y. Ong and E. Y. Liya, *Biomaterials*, 2010, 31, 9023-9030.
10. J. P. Novak, C. Nickerson, S. Franzen and D. L. Feldheim, *Analytical chemistry*, 2001, 73, 5758-5761.

11. I. Sondi and B. Salopek-Sondi, *Journal of colloid and interface science*, 2004, 275, 177-182.
12. N. Jain, A. Bhargava, S. Majumdar, J. Tarafdar and J. Panwar, *Nanoscale*, 2011, 3, 635-641.
13. B. Reidy, A. Haase, A. Luch, K. A. Dawson and I. Lynch, *Materials*, 2013, 6, 2295-2350.
14. K. N. Thakkar, S. S. Mhatre and R. Y. Parikh, *Nanomedicine: Nanotechnology, Biology and Medicine*, 2010, 6, 257-262.
15. S. Iravani, *International Scholarly Research Notices*, 2014, 2014.
16. T. Klaus, R. Joerger, E. Olsson and C.-G. r. Granqvist, *Proceedings of the National Academy of Sciences*, 1999, 96, 13611-13614.
17. N. Saifuddin, C. W. Wong and A. A. Yasumira, *Journal of Chemistry*, 2009, 6, 61-70.
18. K. Kalimuthu, R. S. Babu, D. Venkataraman, M. Bilal and S. Gurunathan, *Colloids and Surfaces B: Biointerfaces*, 2008, 65, 150-153.
19. M. M. G. Babu and P. Gunasekaran, *Colloids and Surfaces B: Biointerfaces*, 2009, 74, 191-195.
20. S. Priyadarshini, V. Gopinath, N. M. Priyadharsshini, D. MubarakAli and P. Velusamy, *Colloids and Surfaces B: Biointerfaces*, 2013, 102, 232-237.
21. M. F. Lengke, M. E. Fleet and G. Southam, *Langmuir*, 2007, 23, 2694-2699.
22. A. R. Shahverdi, A. Fakhimi, H. R. Shahverdi and S. Minaian, *Nanomedicine: Nanotechnology, Biology and Medicine*, 2007, 3, 168-171.
23. M. Arakha, M. Saleem, B. C. Mallick and S. Jha, *Scientific reports*, 2015, 5.
24. S. Liu, G. Huang, J. Yu, T. W. Ng, H. Y. Yip and P. K. Wong, *ACS applied materials & interfaces*, 2014, 6, 2407-2414.
25. W. K. Jung, H. C. Koo, K. W. Kim, S. Shin, S. H. Kim and Y. H. Park, *Applied and environmental microbiology*, 2008, 74, 2171-2178.
26. R. H. Sedlak, M. Hnilova, C. Grosh, H. Fong, F. Baneyx, D. Schwartz, M. Sarikaya, C. Tamerler and B. Traxler, *Applied and environmental microbiology*, 2012, 78, 2289-2296.
27. F. Reith, B. Etschmann, C. Grosse, H. Moors, M. A. Benotmane, P. Monsieurs, G. Grass, C. Doonan, S. Vogt and B. Lai, *Proceedings of the National Academy of Sciences*, 2009, 106, 17757-17762.
28. R. Ramanathan, M. R. Field, A. P. O'Mullane, P. M. Smooker, S. K. Bhargava and V. Bansal, *Nanoscale*, 2013, 5, 2300-2306.
29. R. Ramanathan, A. P. O'Mullane, R. Y. Parikh, P. M. Smooker, S. K. Bhargava and V. Bansal, *Langmuir*, 2010, 27, 714-719.
30. M. J. Ahmed, G. Murtaza, A. Mehmood and T. M. Bhatti, *Materials Letters*, 2015, 153, 10-13.
31. D. D. Evanoff and G. Chumanov, *ChemPhysChem*, 2005, 6, 1221-1231.
32. V. L. Colvin and K. M. Kulinowski, *Proceedings of the National Academy of Sciences*, 2007, 104, 8679-8680.
33. F. X. Schmid, *Encyclopedia of Life Science*, 2001, 1-4.
34. Z. Sadowski, 2010.
35. A. Gupta, P. Singh and C. Shivakumara, *Solid State Communications*, 2010, 150, 386-388.
36. H. Kumar and R. Rani, *Int J Engg Inno Technol*, 2013, 3, 344-348.
37. H. Salem, K. Eid and M. Sharaf, *International Journal of Drug Delivery*, 2011, 3, 293-304.
38. A. Saeb, A. S. Alshammari, H. Al-Brahim and K. A. Al-Rubeaan, *The Scientific World Journal*, 2014, 2014.
39. A. Gole, C. Dash, V. Ramakrishnan, S. Sainkar, A. Mandale, M. Rao and M. Sastry, *Langmuir*, 2001, 17, 1674-1679.
40. N. Goswami, R. Saha and S. K. Pal, *Journal of Nanoparticle Research*, 2011, 13, 5485-5495.
41. C. G. Kumar and S. K. Mamidyala, *Colloids and Surfaces B: Biointerfaces*, 2011, 84, 462-466.
42. C. A. Schneider, W. S. Rasband and K. W. Eliceiri, *Nature methods*, 2012, 9, 671-675.

## Figure legends

Fig. 1. AgNO<sub>3</sub> MIC against *B. thuringiensis*. (a) Bar diagram of O.D. at 600 nm for the culture grown in presence of varying AgNO<sub>3</sub> concentrations, (b) the Baclight fluorescence images of the intact cells (b-I) and the cells grown in presence of 0.15 mM AgNO<sub>3</sub> (b-II).

Fig. 2. (a) UV-Vis spectra of different batch cultures demonstrating the synthesis of AgNP (peak at 414 nm), (b) ATR-FTIR spectra confirming the presence of AgNP in different batch cultures (peaks in the range of 800-500 cm<sup>-1</sup>) and proteins (peaks at 1552 and 1650 cm<sup>-1</sup>).

Fig. 3. Baclight fluorescence images of *B. thuringiensis* obtained from the end of different batch culture containing 0.15 mM AgNO<sub>3</sub> (a-batch 1, b-batch 2, and c-batch 3).

Fig. 4. UV-Visible absorption spectra of fabricated AgNP.

Fig. 5. Hydrodynamic size analysis of AgNP before and after SEC.

Fig. 6. FE-SEM micrographs of (a) *B. thuringiensis* (control, inset image indicate the high magnification image of the surface), (b) *B. thuringiensis* grown in presence of 0.15 mM AgNO<sub>3</sub>, (c) purified fabricated AgNP from elution 2.

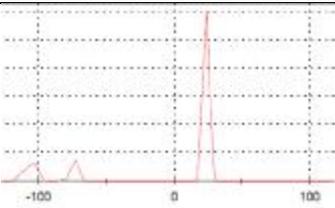
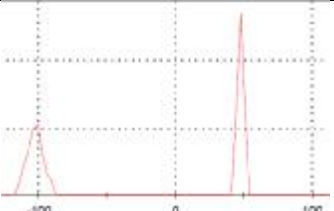
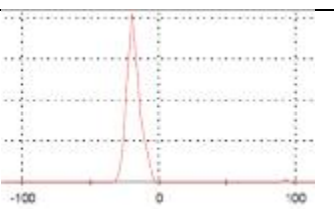
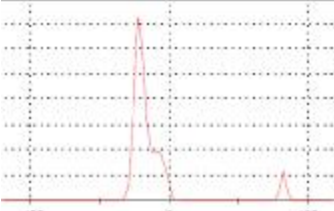
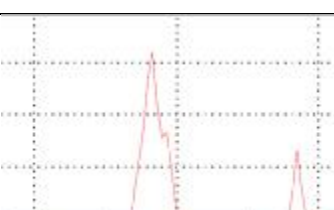
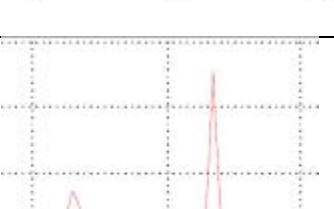
Fig. 7. TEM images of AgNPs. (a) before SEC, (b) elution 1, (c) elution 2, (d) elution 3. The scale bar represents 50 nm.

Fig. 8. ATR-FTIR spectra of suspension before size exclusion chromatographe and of the elutions after the chromatograph.

Fig. 9. Fluorescence microscopic images of (a) intact *E. coli*, and (b) purified fabricated AgNP *E. coli*.

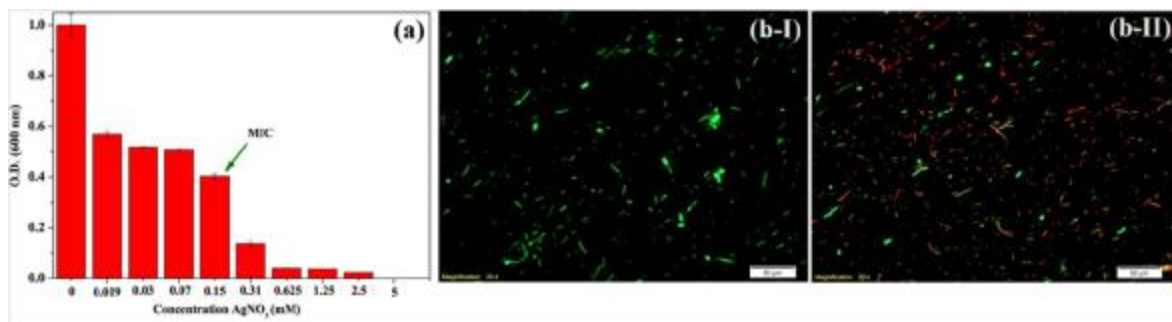
Scheme 1. Schematic diagram elucidating the mechanism of AgNP fabrication.

Table 1. Zeta potential analysis of AgNP before and after the SEC (elution 1-5)

Sample	Zeta potential (mV)	Zeta Graph
Before	23.7 +/- 2.28 (73.8%)	
	-106 +/- 4.47 (15.1 %)	
SEC	-73.3 +/- 3.16 (11 %)	
	-100 +/- 5.8 (47.4 %)	
Elution 1	47.5 +/- 2.26 (52.6%)	
	-100 +/- 5.8 (47.4 %)	
Elution 2	-18.2 +/- 4.75 (99.5 %)	
Elution 3	82.3 +/- 1.94 (5.6%)	
	-20.0 +/- 4.96 (76.3%)	
	-5.89 +/- 3.36 (18.0%)	
Elution 4	84.7 +/- 2.22 (12.3 %)	
	-18.4 +/- 5.11 (64.6%)	
	-7.18 +/- 2.9 (22.9 %)	
Elution 5	34.6 +/- 2.26 (64.1%)	
	-67.5 +/- 4.96 (34.7%)	
	-40.9 +/- 4.00 (1.2%)	

## Figures

Figure 1



**Figure 2**

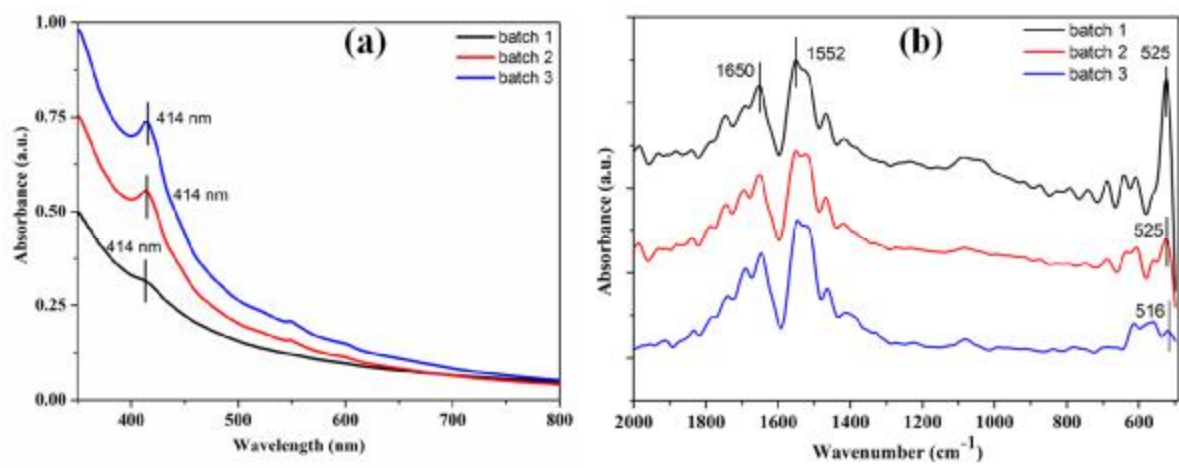


**Figure 3**

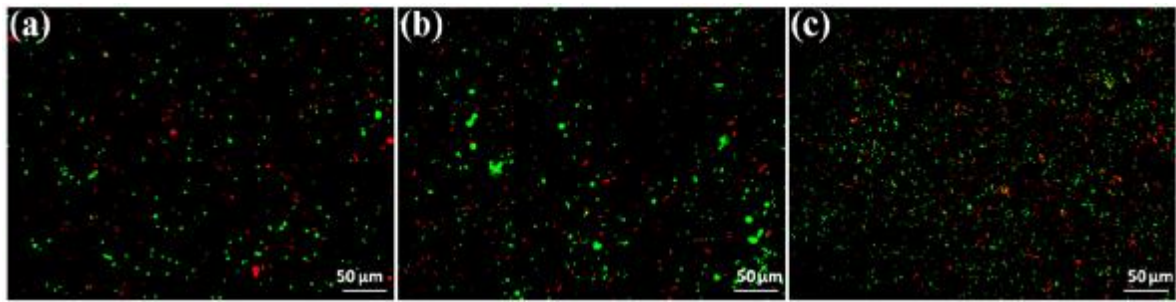


Figure 4

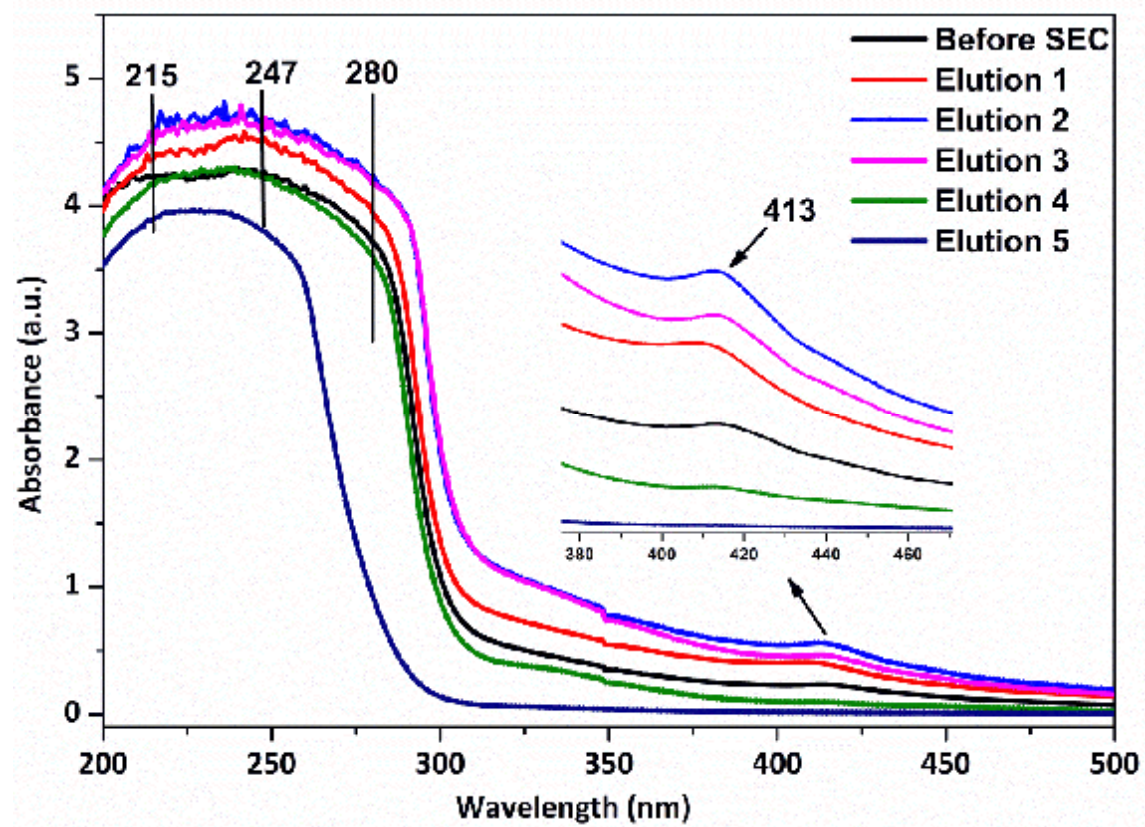
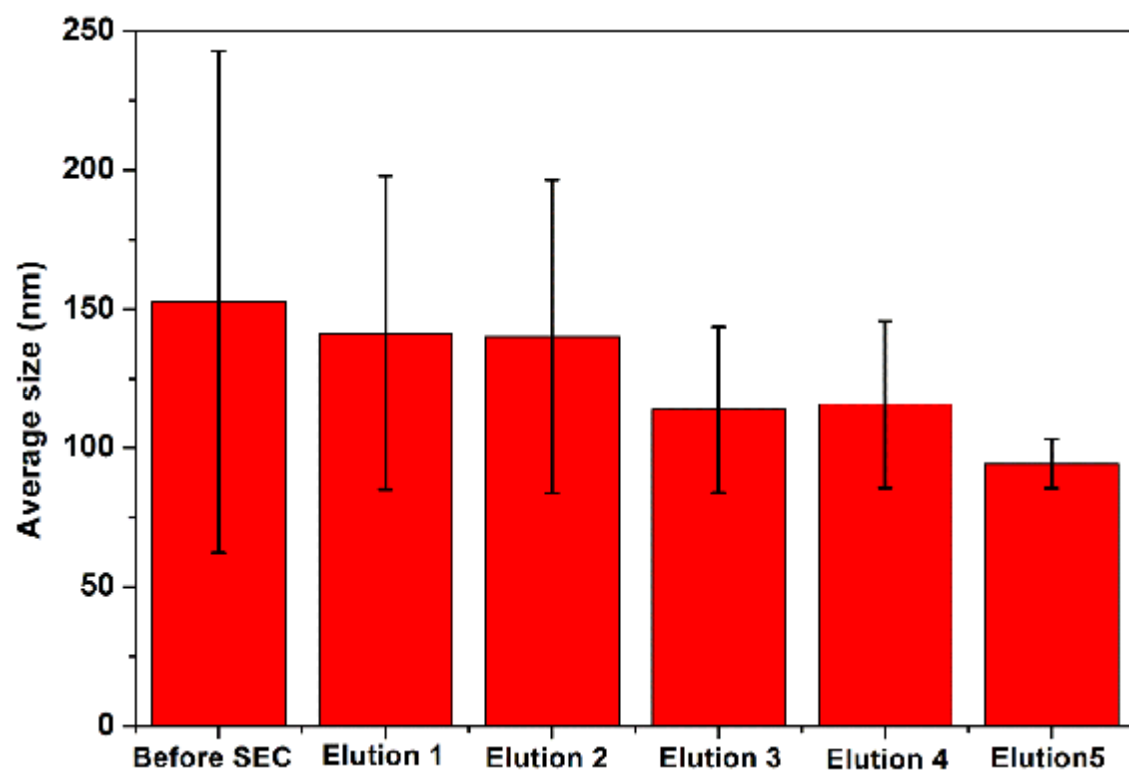


Figure 5



**Figure 6**

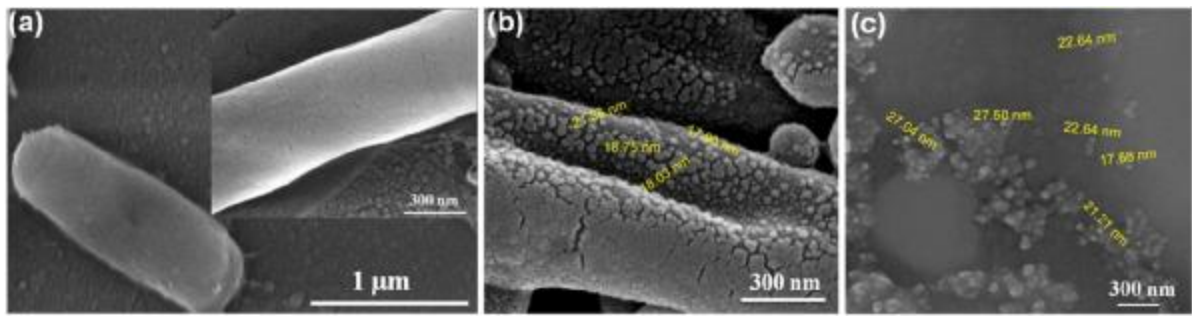


Figure 7

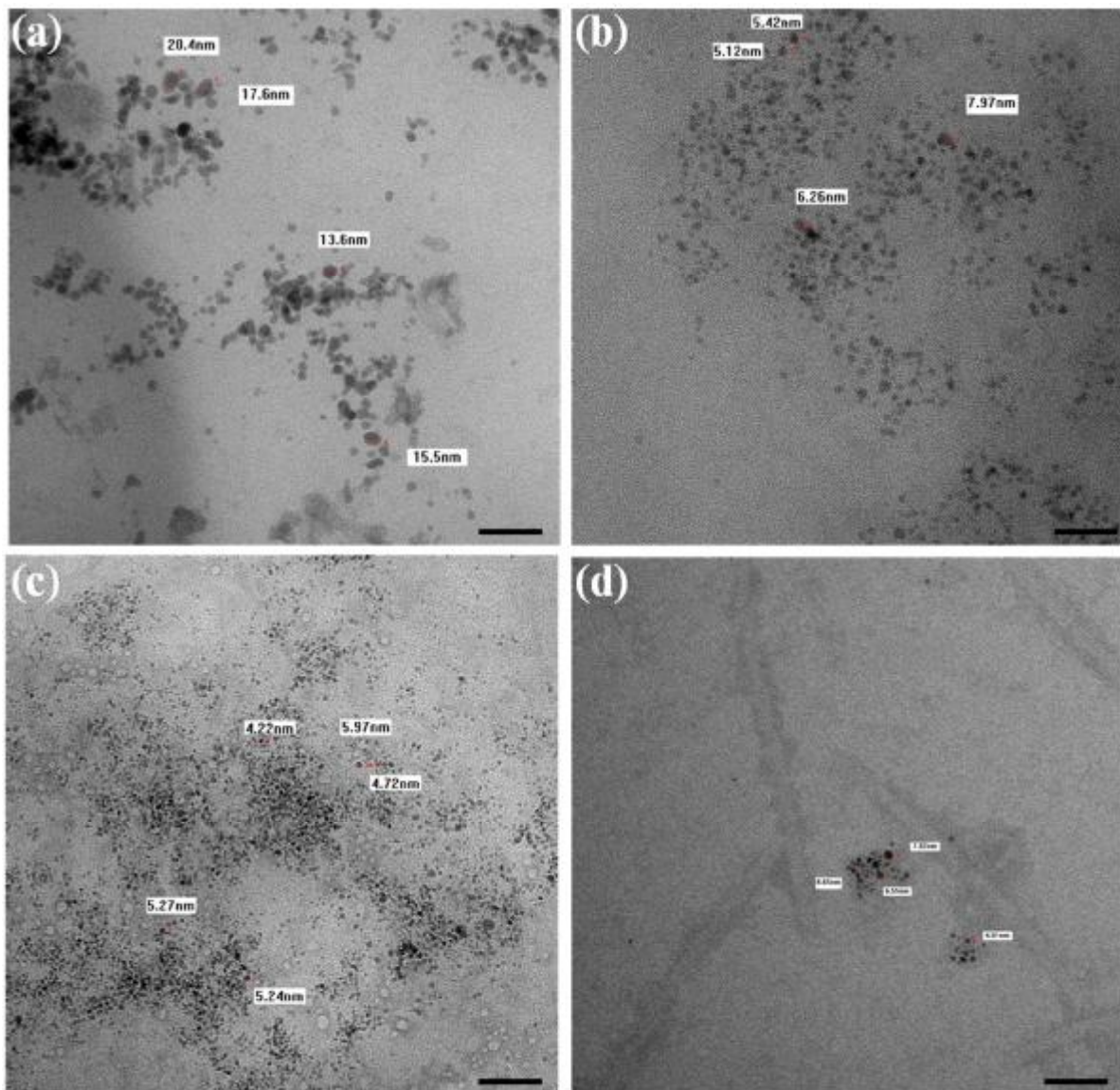
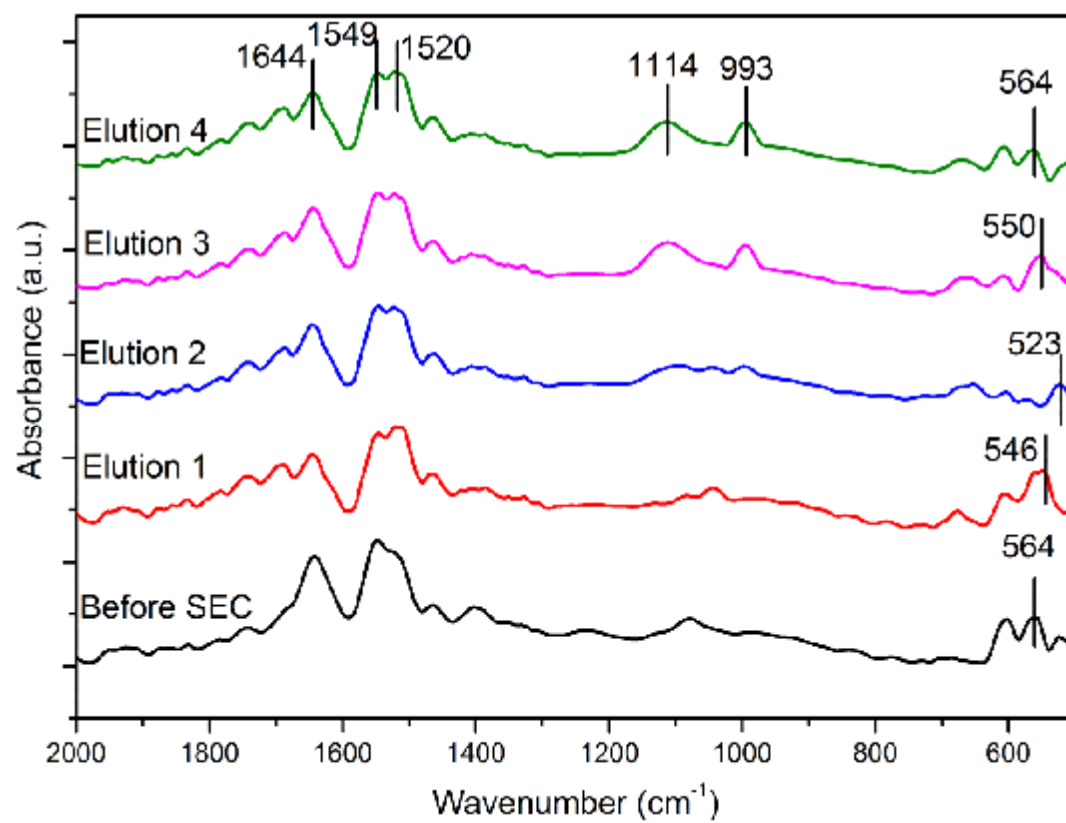
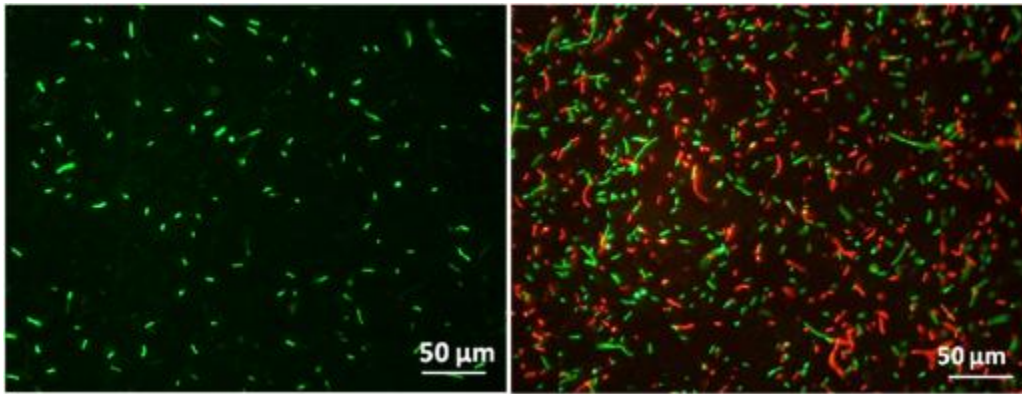


Figure 8



**Figure 9**



Scheme 1

